A&A 409, 781–786 (2003)
DOI: 10.1051/0004-6361:20031100

Astronomy & Astrophysics

Determination of the Ni XVIII plasma recombination rate coefficient

M. Fogle[1], N. R. Badnell[2], N. Eklöw[1], T. Mohamed[1], and R. Schuch[1]

[1] Department of Atomic Physics, Stockholm University, SE106 91 Stockholm, Sweden
[2] Department of Physics, University of Strathclyde, Glasgow G4 0NG, UK

Received 18 March 2003 / Accepted 11 July 2003

Abstract. The absolute radiative and dielectronic recombination rate coefficients for Ni XVIII were measured at the CRYRING storage ring for the center-of-mass energy range 0–43 eV, which covers all $\Delta n = 0$ core excitations up to the $3p_{1/2}$ and $3p_{3/2}$ series limits. These are compared to an AUTOSTRUCTURE intermediate coupling calculation. The absolute rate coefficients are then convoluted with a Maxwellian temperature distribution to obtain the temperature dependent plasma recombination rate coefficient for the temperature range 10^3–10^7 K. The temperature dependent rate coefficient can be useful as a tool in both astrophysical and laboratory plasma diagnostics where the knowledge of ionization balance and level populations are of interest in deciphering the many emission lines observed and for the evaluation of the plasma temperature via emission line ratios.

Key words. atomic data

1. Introduction

Elemental emission lines are nearly a ubiquitous part of cosmic observation, having been observed in astrophysical plasmas from all reaches of the cosmos. Of particular importance are those emission lines which provide diagnostic information, e.g., plasma temperature, paramount in extracting meaningful information from *any* set of emission lines. A quintessential technique employed for temperature diagnostics makes use of line ratios between dielectronic recombination (DR) satellite lines and collisionally-driven resonance lines (Sylwester et al. 1980; Flower & Nussbaumer 1975).

Once the temperature has been established, the recombination rate becomes important in determining the ionization balance and level populations responsible for the emission lines observed. These rates, however, are not always known and thus the analysis makes use of theoretical calculations to simulate the recombination processes. Many of these theoretical tools are based on atomic data and have been shown to represent experimental line shapes and strengths to an exceptional degree of accuracy, however the atomic data used to model such theoretical tools is sparse and there is a continued effort to obtain experimental recombination rate coefficients for various ion species in order to verify the outcome of these theoretical tools.

The most prominent technique for measuring absolute recombination rate coefficients, as a function of center-of-mass (CM) energy, utilizes storage rings coupled with electron coolers (Savin et al. 2002; Schuch 1993; Müller & Wolf 1997; Schippers 1999). These devices have been highly successful in providing a diverse range of ion species and charge states. Here we will concentrate on the radiative recombination (RR) and DR processes undergone by the Na-isoelectronic ion Ni^{17+}. The RR process can be described as

$$e^- + Ni^{17+} \rightarrow Ni^{16+} + h\nu. \tag{1}$$

This is a direct, nonresonant, recombination channel in which a continuum electron is captured by an ion with the subsequent release of a photon.

The resonant $\Delta n = 0$ DR process can be described as

$$\begin{aligned} e^- + Ni^{17+}(3s) &\rightarrow \begin{cases} Ni^{16+**}(3p\,nl) & \text{(i)} \\ Ni^{16+**}(3d\,nl) & \text{(ii)} \end{cases} \\ \text{(i)} &\rightarrow \begin{cases} Ni^{16+*}(3s\,nl) + h\nu \\ Ni^{16+*}(3p\,n'l') + h\nu \end{cases} \\ \text{(ii)} &\rightarrow \begin{cases} Ni^{16+**}(3p\,nl) + h\nu \rightarrow \text{(i)} \\ Ni^{16+*}(3d\,n'l') + h\nu \end{cases} \end{aligned} \tag{2}$$

where the first step is associated with the simultaneous capture of an electron to a Rydberg state (nl), and the excitation of a core electron forming a doubly excited state (**). The subsequent step involves the radiative de-excitation of the ion to a singly excited state (*) below the autoionization threshold. This can occur in one of two manners; the excited core electron relaxes or, the captured Rydberg (nl) electron decays to some other state ($n'l'$). Due to the requirements of energy conservation, DR can only occur at electron energies, E_e,

$$E_e \simeq E_\infty + E_{nl} \tag{3}$$

where E_∞ is the 3s → 3p (3d) excitation energy and E_{nl} is the energy of the recombined electron in the nl state. The energy-dependent RR and DR rate coefficients are convoluted with

Send offprint requests to: R. Schuch,
e-mail: schuch@physto.se

Maxwellian distributions for a temperature range of 10^3–10^7 K to obtain temperature dependent rate coefficients which are useful for plasma diagnostics.

Various species of Ni ions have been observed in high temperature plasmas, e.g., active solar regions (Vernazza & Reeves 1978; Sadlin et al. 1986; Widing et al. 1971) and tokomak test fusion plasmas (Janev 1991; Peacock et al. 1984). While typically less predominant than other lines, they can be used for some of the diagnostics mentioned above and incorporated into existing codes used to model the recombination processes. Using the data of Arnaud & Rothenflug (1985) it can be seen that the mean charge of Ni in a plasma changes from 9+ to 21+ over the temperature range of 10^6–10^7 K which suggests that Ni ions can be used as a sensitive temperature probe over this region.

2. Experiment

The measurement was carried out at the heavy-ion storage ring CRYRING of the Manne Siegbahn Laboratory in Stockholm. Ni^{17+} ions were produced by an electron beam ion source and preaccelerated to 300 keV/amu in a radio frequency quadrapole before injection into the ring. The ions were accelerated to a final energy of 12 MeV/amu and cooled by a velocity-matched electron beam. This resulted in 1.25×10^6 ions stored in the ring per injection. The ion velocity was determined from the Schottky frequency, f_s, of the circulating ions and the ion beam circulating circumference, $L_r = 51.63$ m, by $v_i = f_s L_r$.

The electron cooler coupled to the storage ring is capable of producing electron beams with transverse temperatures ($k_B T$) of 1 meV and post acceleration longitudinal temperatures of 0.1 meV via magnetic adiabatic expansion to a beam diameter of 40 mm (Danared et al. 2000). The electron density in the cooler interaction region was determined to be 1.85×10^7 cm^{-3}.

The concurrent electron-ion interactions that take place inside the cooler are the primary means of studying recombination. At the velocity-matched, cooling condition, RR is the dominate recombination channel. In order to study DR, the electron cooler cathode potential is varied in a systematic manner such that the relative electron and ion velocities differ (DeWitt et al. 1996; Zong et al. 1997). DR resonances occur when the energy conservation rule of Eq. (3) is satisfied. The resulting measured rate coefficient is a convolution of the DR resonances and the flattened Maxwellian distribution of the electrons, given by the different longitudinal and transversal temperature distributions mentioned above, and must be convoluted further to obtain a typical Maxwellian rate coefficient. Charge changed ions are separated by the dipole magnet following the electron cooler section of the ring and then detected by means of a unity efficiency surface barrier detector as a function of the varied cathode potential.

The RR and DR rate coefficients of Ni XVIII were investigated in the energy range up to 43 eV, constituting all $\Delta n = 0$ DR resonances up to the $3s_{1/2} \rightarrow 3p_{1/2}$ and $3s_{1/2} \rightarrow 3p_{3/2}$ series limits. The systematic corrections for space charge and drag force effects where taken in the usual manner (DeWitt et al. 1996). The error in the measured CM energy is estimated at 10 meV, which is derived primarily from the uncertainties in the cathode voltage measurement and the drag force correction. The predominant uncertainties of the measured rate coefficients arise from the determination of the ion current (≈15%) and the uncertainty of the electron-ion interaction length (≈5%).

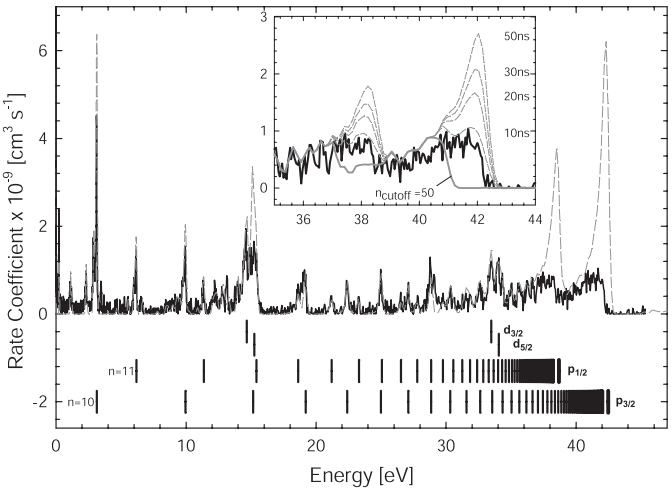

Fig. 1. The experimental DR rate coefficient for the $\Delta n = 0$ transitions up to the $3p_{1/2}$ and $3p_{3/2}$ series limits. The result of an AUTOSTRUCTURE calculation are shown by the dashed curve. The Rydberg series for $3p_{1/2}$ (starting at $n = 11$) and $3p_{3/2}$ (starting at $n = 10$) are illustrated below the curves. A few resonances resulting from $3s_{1/2} \rightarrow 3d_j$ ($j = 3/2, 5/2$) transitions are also indicated. The inlay depicts the series limits region with $n_{cutoff} = 50$ and times of flight results from AUTOSTRUCTURE calculations.

3. Results

3.1. Dielectronic recombination

Figure 1 depicts the measured DR rate coefficient. Using the resonant condition of Eq. (3) and the excitation energies of 38.7 and 42.5 eV, for the $3s_{1/2} \rightarrow 3p_{1/2}$ and $3s_{1/2} \rightarrow 3p_{3/2}$ excitations respectively, the lowest possible recombining Rydberg state for a $3s_{1/2} \rightarrow 3p_{3/2}$ excitation is found to be $n = 10$ and for a $3s_{1/2} \rightarrow 3p_{1/2}$ excitation it is found to be $n = 11$.

As the charge-changed, recombined ions travel from the electron cooler to the detector, they traverse magnet fields ranging from 0.3 T in the torroidal magnets of the electron cooler to 1.2 T in the main dipole magnets. These fields induce a motional electric field which is sufficient to re-ionize electrons which are in high Rydberg states. This is a crucial matter in DR experiments since many of the states created in the recombination process consist of high lying Rydberg electrons and any re-ionization will result in a reduced detection efficiency. The principal quantum state cutoff, above which electrons are re-ionized in a particular field, is determined by

$$n_{cutoff} \simeq \left(6.2 \times 10^{10} \frac{Q^3}{v_i B}\right)^{1/4}, \quad (4)$$

where Q is the charge state of the ion, v_i is the ion velocity, and B is the magnetic field strength. The n_{cutoff} of the dipole magnet was found to be $n_{cutoff} = 50$. The n_{cutoff} effect can clearly be seen at the series limits in Fig. 1. To account for this

cutoff, we have made an AUTOSTRUCTURE (Badnell 1989) intermediate-coupling calculation which is shown in Fig. 1 as a dashed curve overlaying the solid experimental curve. The dramatic rate increase at the series limits shown by the AUTOSTRUCTURE calculation accounts for principal quantum states up to $n = 1\,000$. The $n_{\rm cutoff}$ determined by Eq. (4) does not include any time of flight in which an electron above the $n_{\rm cutoff}$ might decay and thus survive field passage. We have used the AUTOSTRUCTURE result in conjunction with the effective recombination cross section

$$\sigma_{\rm eff}^{nl} = \sigma^{nl}\left[1 - \exp\left(T/\tau\right)\right], \tag{5}$$

where T is the time of flight and τ is the lifetime of the Rydberg state nl. The results of several times of flight from 10–50 ns are illustrated in the inlay of Fig. 1. The AUTOSTRUCTURE result for $n_{\rm cutoff} = 50$ is also shown in the inlay. At the given ion velocity, the flight time to the dipole magnet is expected to be ∼30 ns in which all states above $n = 50$ will be ionized. As can be seen in the inlay of Fig. 1, we clearly see that the $n_{\rm cutoff} = 50$ does not accurately describe the observed behavior at the series limits while a time of flight of 10 ns best describes the experimentally observed $n_{\rm cutoff}$. This can be partially explained by ionization which takes place due to the torroidal magnet. The time of flight from the center of the electron cooler to this magnet is ∼10 ns at which $n_{\rm cutoff} = 71$. This means that only the principal quantum states between 50 and 71 can additionally contribute to the AUTOSTRUCTURE $n_{\rm cutoff} = 50$ result to yield the experimentally observed rate at the series limits. Furthermore, those electrons with low angular momentum will contribute more than those of higher angular momentum since the lifetime of the state increases with angular momentum and thus decreases its probability of decaying before field ionization. A more detailed account of the field ionization for such an experimental arrangement has been taken by Schippers et al. (2001)

The AUTOSTRUCTURE results represent the measured rate coefficient and resonance positions extremely well over the 1–35 eV energy range, thus in determining the plasma rate coefficient we have only used the portion of the AUTOSTRUCTURE results beyond 35 eV as an extrapolation of the experimental rate coefficient. This is termed the *no-field* rate coefficient.

3.2. Radiative recombination

Figure 2 shows the measured RR rate coefficient. As can be seen in the figure, the RR rate falls off rapidly as the CM energy increases. A caveat of the storage ring method is the, yet unexplained, rate enhancement observed in RR as $E_{\rm CM} \rightarrow 0$ (Gao et al. 1995). Since this enhancement effect has not been directly linked to processes which would occur in a natural plasma, we have chosen to fit the experimental results with the RR rate derived from

$$\alpha_n^{\rm RR} = \int \sigma_n^{\rm RR}(E\,(v))\; v\; f(\hat{v}, \boldsymbol{v})\,{\rm d}^3v. \tag{6}$$

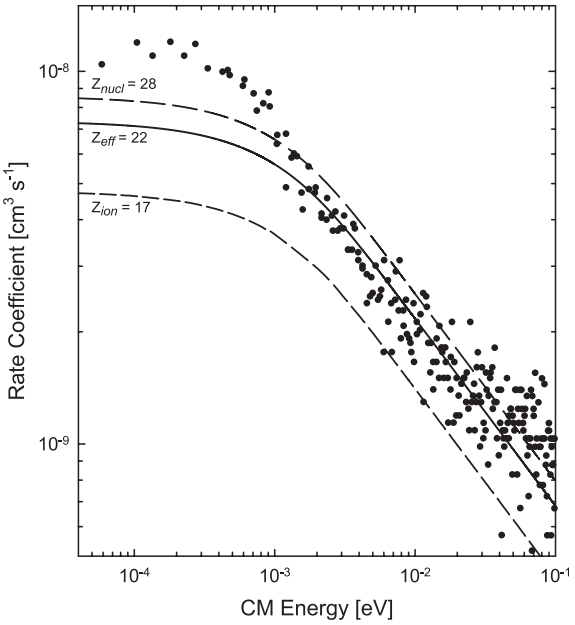

Fig. 2. The experimental RR rate coefficient is represented by the filled-circle symbols. The fit (see text) results are also displayed for various effective Z, including the nuclear charge of 28, the ionic charge of 17, and the resultant fit value of 22.

The Kramers cross section (Kramers 1923) is given by

$$\sigma_n^{\rm RR} = 2.105 \times 10^{-22}\,\Gamma\,\frac{Z^4R^2}{nE(n^2E + Z^2R)}, \tag{7}$$

where Γ is the Gaunt factor used to correct for the semi-classical natural of this expression (Seaton 1959), Z is the effective charge of the ion, R is the Rydberg constant, n is the principle quantum state of recombination, and E is the CM energy. The CM velocity is given by v and $f(\hat{v}, \boldsymbol{v})$ is the flattened Maxwellian velocity distribution of the electrons in the electron cooler (DeWitt et al. 1996). It has been shown in studies of bare ions (Gao et al. 1997), for which the Kramers cross section was initially intended, that the absolute rate coefficients agree with theory perfectly in the region above the transversal temperature of the electron beam and it is in this region we have fit our experimental results.

The RR rate coefficient is also impacted by the $n_{\rm cutoff}$ effect. Therefore, the calculated RR rate coefficient used to fit the experimental data only accounts for states up to $n = 50$. In order to have a hydrogenic description of high-n states, the sum over all $\sigma_n^{\rm RR}$ in Eq. (7) was divided into two discrete parts. For $n = 3$–25, the effective Z was used as the fitting parameter while for $n_{\rm H} > 25$, the ionic charge, i.e., $Z = 17$, was taken; forcing a hydrogenic description of the states. This resulted in an effective $Z = 22$ for $n = 3$–25. One should keep in mind that choosing the $n_{\rm H}$ at which to divide the sum over all cross sections can provide different fitting results, e.g., if $n_{\rm H} = 22$ is used instead, an effective $Z = 25$ for $n < 22$ is necessary to fit the experimental data. The most appropriate $n_{\rm H}$ is suggested from the expression for the effective Z advocated by Hahn (1997),

$$Z_{\rm eff} \simeq \frac{Z_{\rm C} + Z}{2} \quad \text{for} \quad Z > \frac{Z_{\rm C}}{2}, \tag{8}$$

where Z_C is the nuclear charge and Z is the ionic charge. This expression yields $Z_{\rm eff} = 22.5$ while the fit to the data yields $Z_{\rm eff} = 22$. In determining the plasma rate coefficient, we have taken the effective $Z = 22$ from the fit and extended the theoretical RR rate up to $n = 1000$, using $Z = 17$ for $n_{\rm H} > 25$, so as to be consistent with the range of states covered by the DR no-field rate coefficient.

3.3. Plasma recombination rate

The temperature-dependent plasma recombination rate coefficient is determined by

$$\alpha(T_{\rm e}) = \int \alpha(E)\ f(E, T_{\rm e})\ {\rm d}E \tag{9}$$

where $\alpha(E)$ is the energy-dependent rate coefficient measured in the experiment and

$$f(E, T_{\rm e}) = \frac{2\,E^{1/2}}{\pi^{1/2}\,(k_{\rm B}T_{\rm e})^{3/2}}\ \exp\left(-\frac{E}{k_{\rm B}T_{\rm e}}\right), \tag{10}$$

where E is the CM energy and $T_{\rm e}$ is the electron temperature, is a Maxwellian distribution. Temperatures in the range of 10^3–10^7 K were used in the convolution. Figure 3 shows the result of this convolution for the no-field (thick solid curves) and experimental (long-dashed curves) RR and DR rate coefficients. The RR rate coefficient falls off rapidly as temperature increases and, in the no-field case, DR becomes the dominant recombination channel after ~20 000 K. The DR portion of the data was separated from RR at 1 eV and the above convolution for the DR plasma recombination rate coefficient only used the DR resonances above this energy, including the AUTOSTRUCTURE extrapolation. For comparison, the pure AUTOSTRUCTURE rate coefficient results for both RR and DR with $n_{\rm cutoff} = 1000$ are also shown in Fig. 3 (thin solid curves).

The resulting RR and DR rate coefficients are compared to theoretical expressions derived from various fits to experimental and theoretical data involving many different ions. These fits for high Z ions are typically the result of extrapolation along isosequences and this is prevalent for the fit parameters used to describe the recombination rate coefficient of Ni XVIII.

The semi-empirical expression devised by Burgess (1965) for the DR rate coefficient has been widely used for many ions. The result of the Burgess formula for Ni XVIII is shown in Fig. 3 (dotted curve). The oscillator strengths given by Weiss (1977) and the excitation energies mentioned in Sect. 3.1 have been used. This result describes the peak DR rate obtained from the no-field rate coefficient rather well, however, as with all of the theories compared, except AUTOSTRUCTURE, it falls shorts of representing the low temperature ($<10^5$ K) DR rate.

Mewe et al. (1980) also derived simple semi-empirical expressions for both RR and DR. The results of these expressions are shown in Fig. 3 (short-dashed curves) for both the RR and DR rate coefficients. The RR result of Mewe et al. has been calculated utilizing the effective $Z = 22$ found in the RR fit of the experimental data. Using the ionic charge $Z = 17$ yields an RR rate 55.5% lower. As can be seen in Fig. 3, the $Z = 22$ result represents the experimental RR result above 5×10^4 K rather well but diverges to an RR rate ~60% higher than the experimentally derived rate at 10^3 K. The DR result of Mewe et al. is approximately a factor of 3 lower than the no-field experimental result at the peak value, however, it begins to converge with the experimental results at 4×10^6 which, in the low density limit, is where Ni XVIII will have the maximum ionization fraction. Mewe et al. point out that the incorporation of autoionization effects in their expression can, for some ions, result in DR rate coefficients substantially below those from the Burgess formula.

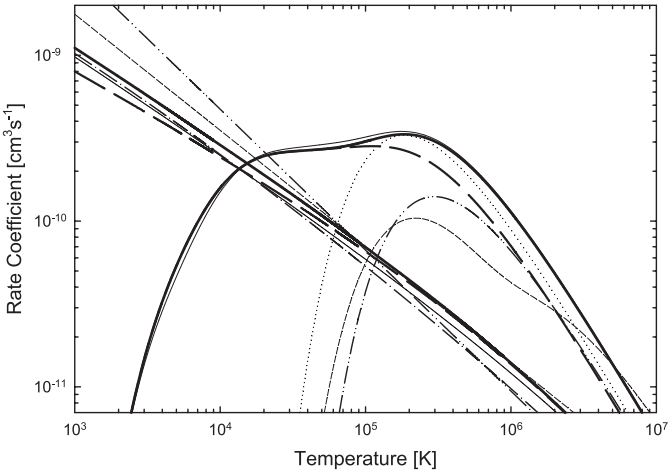

Fig. 3. The RR and DR plasma recombination rate coefficients. The thick solid curves represent the results for RR and DR from the no-field data as discussed in the text. The experimental DR and $n_{\rm cutoff} = 50$ RR rate coefficients are shown as long-dashed curves. The AUTOSTRUCTURE $n_{\rm cutoff} = 1000$ result for both RR and DR are shown as thin solid curves. The dotted curve represents the DR rate coefficient of Burgess (1965), the short-dashed curves represent the RR and DR rate coefficients of Mewe et al. (1980), the dash-dot-dot curves represent the RR and DR rate coefficients of Shull & van Steenberg (1982), and the dash-dot curve represents the RR rate coefficient of Verner & Ferland (1996).

Shull & van Steenberg (1982) have derived expressions and fit parameters for both RR and DR rate coefficients. The RR expression is based on interpolation along isosequences from the data of Aldrovandi & Péquignot (1976) (Mg II ($3.3 \times 10^2 < T < 10^5$ K), Si IV ($10^3 < T < 3 \times 10^5$ K), S VI ($3.3 \times 10^3 < T < 10^6$ K)) and Woods et al. (1981) (Fe XVI ($6.1 \times 10^5 < T < 9.7 \times 10^6$ K)). The DR expression is a least-squares fit to the calculated values of Jacobs et al. (1980). The results for Ni XVIII are shown in Fig. 3 (dash-dot-dot curves). The RR rate coefficient falls off at a higher rate than any of the other theories compared, however, it approximately predicts the same temperature at which DR becomes the dominant recombination channel, as compared to the experimental results (15 000–20 000 K). The observed divergence from the other RR rate coefficients below 10^4 K can possibly be attributed to a combination of flawed data and adverse effects caused by fitting outside the temperature validity ranges indicated for each ion. The DR rate coefficient is about a factor of 2.5 less than the peak no-field DR rate and peaks at a temperature 10^5 K higher. At high temperatures beyond the peak value, the DR rate tends to follow the experimental result.

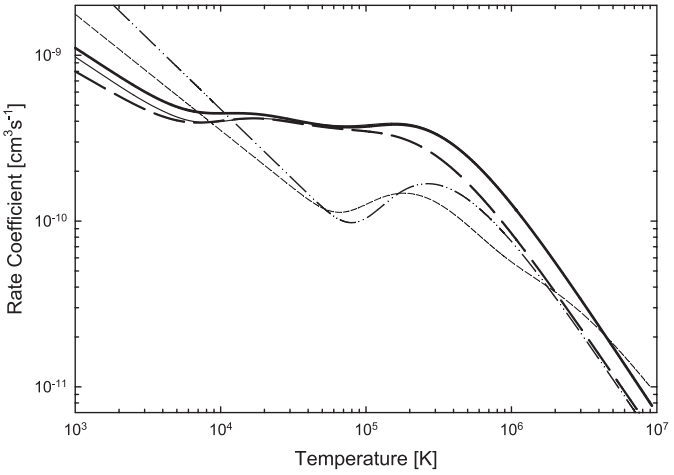

Fig. 4. The total plasma recombination rate coefficient. The thick solid curve is the sum of the no-field RR and DR rate coefficients shown in Fig. 3. The thin solid curve is the total rate coefficient from the AUTOSTRUCTURE $n_{\rm cutoff} = 1000$ calculation for RR and DR. The long-dashed curve represents the experimental rate coefficient (corresponding to the 10 ns time of flight in the inlay of Fig. 1). The short-dashed curve is the sum of the RR and DR rate coefficients of Mewe et al. (1980) and the dash-dot-dot curve is the sum of the RR and DR rate coefficients of Shull & van Steenberg (1982).

The results of Verner & Ferland (1996) for the RR rate coefficient are shown in Fig. 3 (dash-dot curve). Verner & Ferland use the ionic charge in their representation of the fit parameters for various ions. If one extrapolates their result for Na-isoelectronic ions, it is found that an effective $Z = 20$ yields a rate consistent with the no-field RR rate coefficient found for Ni XVIII at 10^4 K. At low temperature, the RR rate of Verner & Ferland is in good agreement with both the result from AUTOSTRUCTURE $n_{\rm cutoff} = 1000$ and the experimental RR result. In this region high-l contributions to the rate are more pronounced. In the high temperature regime, where high-l contributions are not as significant, Verner & Ferland disagree more with the AUTOSTRUCTURE and experimental RR results, with the AUTOSTRUCTURE result tending more towards the experimental no-field rate coefficient. The AUTOSTRUCTURE RR calculation used the distorted wave method for all n and $l = 0$–3 and a Coulomb description for $l > 3$. This was taken up to $n = 1\,000$ and $l = 200$. If a Coulomb description is taken also for $l = 0$–3, for $n > 5$ as used by Verner & Ferland, a similar result to theirs is obtained.

The total recombination rate coefficient is derived by summing the respective RR and DR contributions. Figure 4 illustrates the resulting total recombination rate coefficients. The results obtained from the sum of the RR and DR experimental and no-field curves from Fig. 3 are compared to the sum of the RR and DR rate coefficients of the AUTOSTRUCTURE $n = 1000$ results, Mewe et al. (1980), and Shull & van Steenberg (1982). As can be seen in Fig. 4, the most dramatic difference is that caused by the extra DR information obtained from the experiment for temperatures below 10^5 K. This nonetheless is an accurate representation of the total rate coefficient since it includes all of the various states involved in the recombination process.

Table 1. Ni XVIII $\Delta n = 0$ plasma DR rate coefficient fit parameters to Eq. (11). The fit is to the experimental (long-dashed curve) and the no-field (thick full curve) DR rate coefficients in Fig. 3. The fit results are accurate to within 0.3% above 4000 K.

	No-field		Exp.	
i	c_i (cm^3 s^{-1} K$^{3/2}$)	E_i (eV)	c_i (cm^3 s^{-1} K$^{3/2}$)	E_i (eV)
1	2.70×10^{-4}	1.23	2.61×10^{-4}	1.22
2	2.63×10^{-3}	2.88	2.54×10^{-3}	2.84
3	5.27×10^{-3}	7.46	4.52×10^{-3}	7.00
4	2.57×10^{-2}	16.69	2.39×10^{-2}	15.80
5	1.31×10^{-1}	38.41	6.64×10^{-2}	35.64

Finally, we have fit the experimental and no-field DR rate coefficients in Fig. 3 to the equation

$$\alpha(T_{\rm e}) = T_{\rm e}^{-3/2} \sum_i c_i \exp\left(-\frac{E_i}{k_{\rm B} T_{\rm e}}\right) \quad (11)$$

where E_i and c_i are paremeters related to the excitation energy and oscillator strength, respectively. This expression is of the same general form as the Burgess formula (Burgess 1965), i.e., it has the same $T^{-3/2}$ dependence. Table 11 indicates the fit parameters which are accurate to within 0.3% above 4000 K. Below 4000 K the accuracy lessens to within 20%, however, this is somewhat unimportant since below ~20 000 K, RR is the dominant recombination channel.

4. Conclusions

The absolute RR and DR recombination rate coefficients for Ni XVIII have been determined from a storage ring recombination experiment over the temperature range 10^3–10^7 K. All $\Delta n = 0$ transitions over the 0–43 eV energy range have been investigated. The $n_{\rm cutoff}$ induced by motional electric fields from the torriodal and dipole magnets have been investigated and an AUTOSTRUCTURE calculation has been performed to account for this field ionization. The experimental RR and DR rate coefficients were convoluted with a Maxwellian distribution in order to determine the temperature dependent plasma recombination rate coefficients. These plasma rate coefficients were compared to several theoretical expressions for both the RR and DR rate coefficient. The peak DR rate coefficient is well described by the Burgess (1965) formula, however, the AUTOSTRUCTURE result is a better representation of the overall DR rate given its excellent agreement at low temperature. The experimental and AUTOSTRUCTURE RR results are similar to the RR rate of Verner & Ferland at low temperature while indicating a slighly higher rate at high temperature. The higher rate indication of the AUTOSTRUCTURE calculation approaches the no-field rate and can be regarded with more significance.

The atomic data provided here for Ni XVIII can be used to supplement existing model codes and, with its heightened temperature sensitivity, makes an excellent candidate as a temperature diagnostic line.

Acknowledgements. The authors would like to acknowledge the Swedish Research Council for financial support. We are also grateful for the assistance received from the CRYRING staff at Manne Siegbahn Laboratory. T.M. would like to thank the Egyptian government for financial support.

References

Aldrovandi, S. M. V., & Péquinot, D. 1976, A&A, 47, 321
Arnaud, M., & Rothenflug, R. 1985, A&AS, 60, 425
Badnell, N. R., & Pindzola, M. S. 1989, Phys. Rev. A, 39, 1685
Burgess, A. 1965, ApJ, 141, 1588
Danared, H., Källberg, A., Andler, G., et al. 2000, Nucl. Instrum. Meth A, 441, 123
DeWitt, D. R., Schuch, R., Gao, H., et al. 1996, Phys. Rev. A, 53, 2327
Flower, D. R., & Nussbaumer, H. 1975, A&A, 42, 265
Gao, H., DeWitt, D., Schuch, R., et al. 1995, Phys. Rev. Lett., 75, 4381
Gao, H., Schuch, R., Zong, W., et al. 1997, J. Phys. B: At. mol. Opt. Phys., 30, L499
Hahn, Y. 1997, Rep. Prog. Phys., 60, 691
Jacobs, V. L., Davis, J., Rogerson, J. E., et al. 1980, ApJ, 239, 1119
Janev, R. K. 1991, Phys. Scr., 137, 5
Kramers, H. A. 1923, Philos. Mag., 46, 836
Mewe, R., Schrijver, J., & Sylwester, J. 1980, A&AS, 40, 323
Müller, A. & Wolf, A. 1997, in Accelerator-based atomic physics techniques and applications, ed. J. C. Austin & S. M. Shafroth (Woodbury: AIP Press), 147
Peacock, N. J., Stamp, M. D., & Silver, J. D. 1984, Phys. Scr., T8, 10
Sandlin, G. D., Bartoe, J. D. F., Brueckner, G. E., Tousey, R., & Vanhoosier, M. E 1986, A&A, 61, 801
Savin, D. W., Kahn, S. M., Linkemann, J., et al. 2002, ApJ, 576, 1098
Schippers, S. 1999, Phys. Scr., T80, 158
Schippers, S., Müller, A., Gwinner, G., et al. 2001, ApJ, 555, 1027
Schuch, R. 1993, in Review of Fundamental Processes and Applications of Atoms and ions, ed. C. D. Lin (Singapore: World Scientific), 169
Seaton, M. J. 1959, MNRAS, 119, 81
Shull, J. M., & van Steenberg, M. 1982, ApJS, 48, 95
Sylwester, J, Mewe, R., & Schrijver, J. 1980, A&AS, 40, 335
Vernazza, J. E., & Reeves, E. M. 1978, ApJS, 37, 485
Verner, D. A., & Ferland, G. J. 1996, ApJS, 103, 467
Widing, K. G., Sandlin, G. D., & Cowan, R. D. 1971, ApJ, 169, 481
Weiss, A. W. 1977, J. Quant. Spectrosc. Radiat. Transfer, 18, 481
Woods, D. T., Shull, J. M., & Sarazin, C. L. 1981, ApJ, 249, 399
Zong, W., Schuch, R., Lindroth, E., et al. 1997, Phys. Rev. A, 56, 386